Tectonophysics 864 (2023) 230022

Contents lists available at ScienceDirect

Tectonophysics

journal homepage: www.elsevier.com/locate/tecto

High-resolution scan of the Pyrenean crustal structure combining magnetotelluric and gravity data

P. Piña-Varas [a,*], R. Soto [b], P. Clariana [b], C. Ayala [c], F. Rubio [d], J. Ledo [e], C. Rey-Moral [d], A. Martí [a], G. Mitjanas [a], P. Queralt [a], A. Marcuello [a], P. Santolaria [a], E. Pueyo [b]

[a] Departament de Dinàmica de la Terra i de l'Oceà, Facultat de Ciències de la Terra, Universitat de Barcelona, Barcelona, Spain
[b] Instituto Geológico y Minero de España (CN IGME-CSIC), Unidad de Zaragoza, Zaragoza, Spain
[c] Geosciences Barcelona-CSIC, Barcelona, Spain
[d] Instituto Geológico y Minero de España (CN IGME-CSIC), Madrid, Spain
[e] Departamento de Física de la Tierra y Astrofísica, Facultad de Física, Universidad Complutense de Madrid, Spain

ARTICLE INFO

Keywords:
Magnetotelluric 2D inversion
Gravity modelling
Joint interpretation
La Maladeta massif
Different intrusive pulses

ABSTRACT

The Pyrenees have undergone complex geodynamic evolution starting with experiencing significant tectonic events during the Variscan Orogeny, followed by the intrusion of large granitic complexes during the late Variscan stage, then the collision between the Iberian and European plates during the Alpine Orogeny, and finally, Mesozoic extension. Despite extensive studies and the application of various geophysical methods (two-dimensional seismic reflection data, gravity, and long period magnetotellurics) to investigate the Pyrenean structure, there are still fundamental questions regarding its basement and cover architecture. Specifically, the geometry at depth of significant bodies such as the Late Variscan intrusive granites and Triassic evaporitic accumulations, remains unclear. To better understand these issues, we have conducted joint magnetotelluric and gravity surveys along a 60-km-long transect, spanning the boundary between the Axial and South Pyrenean Zones. Our final geological interpretation shows that the La Maladeta batholith consists of two distinct granitic bodies related to different intrusive pulses. In addition, we identify important Triassic evaporitic accumulations at depth. This work shows the high potential of integrating two geophysical models for understanding the geological evolution of structurally complex areas. The magnetotelluric and gravity data are complementary, with each dataset providing a different resolution for investigating the basement and cover architecture of the Pyrenees. These resolutions depend on the varied petrophysical properties of the rocks involved, including water content and deformation grade.

1. Introduction

The construction of valid and reliable geological models requires the integration of both geological and geophysical data. Numerous studies have demonstrated the effectiveness of combining multiple geophysical techniques with geological data to constrain geological models (e.g., Ayala et al., 2022; Mitjanas et al., 2021; Henke et al., 2020; Le Pape et al., 2017; Pous et al., 1995).

Many geological and geophysical studies have been used to characterize the shallow and deep structure of the Pyrenees (e.g., ECORS-Pyrenees Team, 1988; Muñoz, 1992; Mouthereau et al., 2014; Santolaria et al., 2016; Chevrot et al., 2018, 2022; Ford et al., 2022). Hydrocarbon exploration activities during the 1960s, 1970s, and 1980s have provided a wealth of seismic lines and well data, which have contributed valuable information for understanding the geological structure of the Pyrenean belt. However, there are certain areas—such as the core of the belt with complex structures or regions located between 2-D seismic lines with significant variations along and/or across strike— that still have unresolved geometries at depth. The central area, the Axial Zone, as well as its limit with the South Pyrenean zone, were surveyed by the ECORS-Pyrenees deep seismic reflection profile (e.g., Choukroune and ECORS team, 1989). However, these areas are still poorly constrained by other geophysical datasets.

Numerous and diverse geophysical surveys have been conducted to characterize the structure of the Pyrenees at different scales: from the upper crust to the lithosphere (e.g., Ortuño et al., 2008, 2013; Campanyà

* Corresponding author.
E-mail address: p.pina@ub.edu (P. Piña-Varas).

https://doi.org/10.1016/j.tecto.2023.230022
Received 1 February 2023; Received in revised form 20 August 2023; Accepted 24 August 2023
Available online 4 September 2023

et al., 2011, 2012; Chevrot et al., 2014; Wang et al., 2016; Ledo et al., 2000; Clariana et al., 2022; Soto et al., 2022). Some of these studies have focused specifically on characterizing the basement and cover structures in areas where there is greater uncertainty regarding the subsurface geology (Clariana et al., 2022). However, studies involving a combination of different geophysical datasets (e.g., Rodríguez et al., 2015; García-Yeguas et al., 2017) are less common.

In this study, we integrate magnetotelluric (MT) and gravity surveys with geological and petrophysical data to gain insights into the poorly constrained region of the Pyrenean belt: the boundary between the South-Central-Pyrenees and the Axial Zone near the La Maladeta granitic massif (Fig. 1). By combining these geophysical techniques, we are able to determine the subsurface geometry at depths of up to 10 km. The resulting geophysical models provide valuable information that improves our understanding of the geologic evolution in the study area, in addition to demonstrating the utility of integrating MT and gravity data to constrain geologic models.

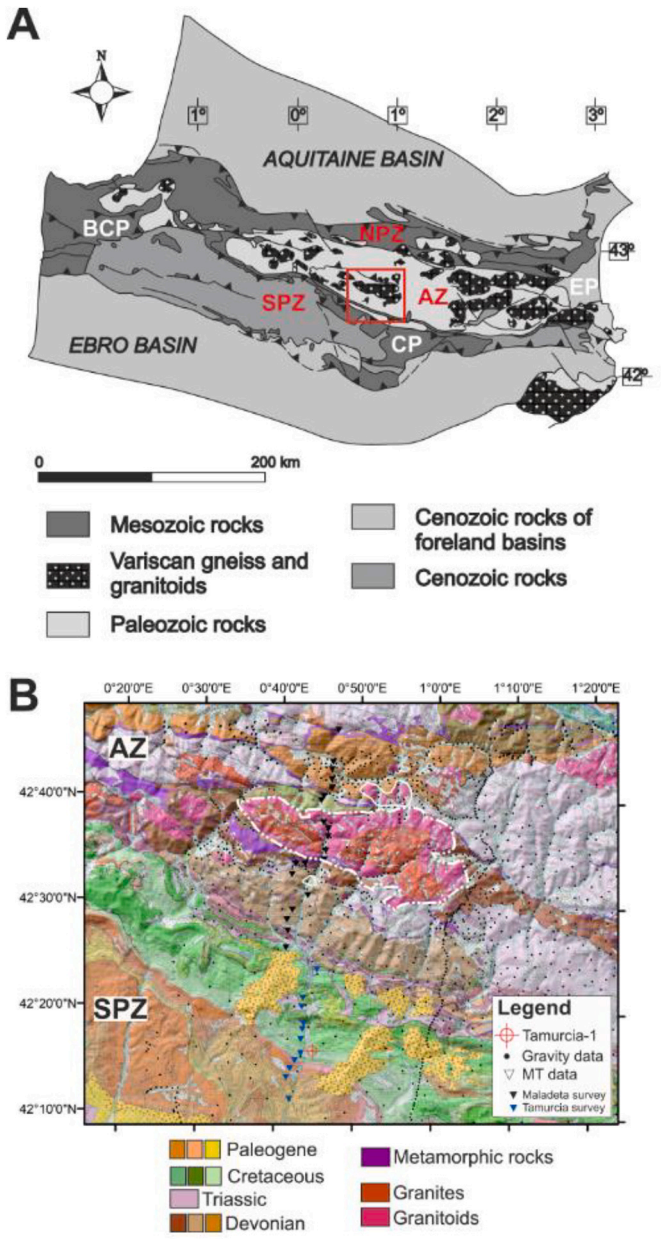

Fig. 1. a) Geological sketch of the Pyrenees. b) Geological map of the study area with La Maladeta Massif highlighted in white. Red box: Study area; NPZ: North Pyrenean Zone; AZ: Axial Zone; SPZ: South Pyrenean Zone; EP: Eastern Pyrenees; CP: Central Pyrenees; BCP: Basque-Cantabrian Pyrenees; Black triangles: MT sites recently acquired; Blue triangles: MT sites acquired in 2006; Black dots: gravity data. White dashed line: La Maladeta granite; White continuous lines: Arties granite in the north and Bono granites in the South. (For interpretation of the references to colour in this figure legend, the reader is referred to the web version of this article.)

1.1. Geological setting

The Pyrenean range is an east-west trending doubly vergent orogenic belt that formed by the collision of the Iberian and European plates during the Alpine Orogeny, which took place from the Late Cretaceous to the Miocene (Roure et al., 1989; Muñoz, 1992; Beaumont et al., 2000; Mouthereau et al., 2014). The range is typically divided into three main areas from east to west: the Eastern Pyrenees, Central Pyrenees, and Basque-Cantabrian Pyrenees, each of which having a different tectonic style that was influenced by factors such as the distribution of Triassic salts (Saura et al., 2016; Ford and Vergés, 2020; Burrel et al., 2021; Izquierdo-Llavall et al., 2020). From north to south, it is also divided into three major zones: the North-Pyrenean Zone, characterized by a thick succession of Mesozoic sedimentary rocks; the Axial Zone, comprising mainly basement rocks, which occur in several thrust sheets, having been deformed during the Variscan orogeny (Middle-Late Carboniferous); and the South-Pyrenean Zone, a fold and thrust belt with a distinct southward vergence, known as the South-Central-Pyrenean zone in the Central Pyrenees.

In general, the rocks that outcrop along the Pyrenean belt can be classified into two types: Pre- and Syn-Variscan basement and Post-Variscan cover. The first group occurs mainly along the Axial Zone and comprises Precambrian and Palaeozoic (Cambrian to Carboniferous) rocks affected by the Variscan orogeny (Fig. 1a). The second group corresponds to Permian to Cenozoic successions, which have been involved in both thick- and thin-skinned tectonic styles across different segments of the orogenic system (Basque-Cantabrian, Central, and Eastern Pyrenees) (Cochelin et al., 2017b; Casas et al., 2019).

Our study area is situated in the Central Pyrenees, specifically at the boundary between the Axial Zone and the South Pyrenean Zone (Fig. 1a, red box). In this region, the Axial Zone is characterized by a thick series of Palaeozoic metasediments that overlie an undifferentiated Neoproterozoic basement. The basement primarily consists of quartzites and slates (Cambro-Ordovician), black shales (Silurian), and slates and limestones (Devonian) (Zwart, 1979; Poblet, 1991; García-Sansegundo et al., 2004, 2011). Late Variscan granitoids in this area are commonly interpreted as products of extensive crustal melting (Barnolas and Chiron, 1996). One of these igneous bodies, La Maladeta granite, widely outcrops. Its emplacement age has been dated to the Late Carboniferous–Early Permian (Evans et al., 1998; Solé et al., 1997). The La Maladeta granite represents one of the largest granitic massifs exposed in the Axial Zone and has been extensively studied, focusing primarily on its petrology and geochemistry (Leblanc et al., 1994; Ubide et al., 2014). However, its subsurface geometry remains poorly constrained. To its south and north, the Bono and Arties granites outcrop, respectively (Fig. 1b).

The South-Central-Pyrenean zone is characterized by the presence of Triassic salts, which act as its main décollement level, playing a significant role in determining deformation processes (Muñoz et al., 2018). As a result, this area exhibits a series of thrusts where the Mesozoic cover is detached from the underlying basement by Triassic evaporites, leading to a thin-skinned deformation style. Within this zone, three major thrust units have been identified (Muñoz, 1992): Bóixols, Montsec, and Sierras Marginales. The Bóixols thrust sheet is the only one located within our study area. The Triassic successions in this region correspond to the Germanic facies, which include Buntsandstein red beds, Muschelkalk dolostones and limestones, and Keuper evaporites and shales. The Jurassic and Cretaceous units mainly consist of thick successions of limestones and marls (García-Senz, 2002; Simó, 2004; Pujalte and

Schmitz, 2005). The Cenozoic rocks are composed of sandstone and limestone, with the youngest deposits comprising Late Paleogene conglomerates.

2. Geophysical data

To obtain a comprehensive geological model of the limit between the South-Central-Pyrenees and the Axial Zone near the La Maladeta massif, we have combined MT and gravity data acquired from different surveys. The geophysical data have been modelled along different profiles based on their distributions, including two gravity profiles and one MT profile (Fig. 2).

2.1. Magnetotelluric data

In the study area, a total of 31 broadband magnetotelluric (BBMT) sites were recorded during two different surveys. In 2006, 11 MT sites were acquired in the southernmost area, focusing on the Bóixols thrust sheet (blue triangles in Fig. 1b). An additional 20 BBMT sites were recorded in 2019 in the northern area to study the La Maladeta granite (black triangles in Fig. 1b). Both datasets were collected along similar NNE-SSW profiles. Herein, we combine these datasets to create a single resistivity model approximately 55 km in length, crossing the La Maladeta granite massif and the boundary between the Axial and the South-Central zones (Fig. 1).

The acquisition of MT data in the study area presented challenges due to the rugged topography, which limited access to possible measurement points. As a result, some of the sites accessed had poor data quality due to local cultural noise. Consequently, several MT sites had to be discarded, reducing the final number of sites used for the inversion model to 21.

For the MT data, the impedance tensor components (Z) were obtained for a period range of 0.001 to 10 s. The regional strike direction was determined using the multi-site, multi-frequency MT tensor decomposition code developed by McNeice and Jones (2001), based on the Groom and Bailey scheme (Groom and Bailey, 1989). This analysis helps to detect and eliminate distortions caused by small near-surface inhomogeneities. Fig. 2 illustrates the strike directions estimated from

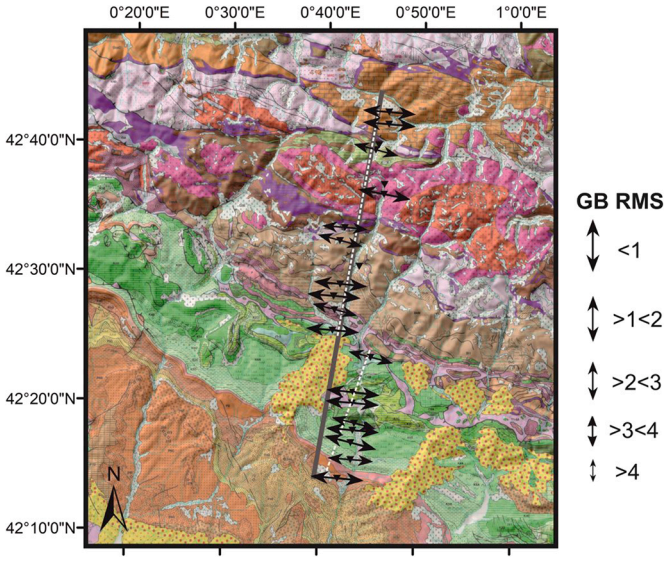

Fig. 2. Geological map of the study area (See Fig. 1b for geological legend). Arrows correspond to geoelectric strike direction obtained for the periods 0.001–10 s at each MT site scaled by the inverse of the error (see text for details). MT sites are located at the centre of each arrow. White dashed lines: gravity profiles (Maladeta section in the north and Boixols section in the south); Grey continuous line: MT profile.

Z at each site within the considered period range (0.001–10 s), using an error floor of 5%. The symbols in Fig. 2 are scaled by the misfit to the Groom and Bailey distortion model. Misfits with an RMS larger than 2.0 indicate three-dimensional effects. In this case, the overall behaviour shows a misfit below 2.0, suggesting that a 2-D model is appropriate. We determined the best-fit average multi-site, multi-frequency regional strike to be N100°E for the complete dataset, which aligns with the observed strike of major geological structures. Consequently, the data were rotated to match this strike direction.

Simultaneous 2-D inversions of the TM and TE mode apparent resistivities and phases were conducted using the algorithm developed by Rodi and Mackie (2001) and implemented in Schlumberger's WingLink software®. The inversions were performed for a period range of 0.001 to 10 s. The initial model used for the inversions was a uniform half-space with a resistivity of 100 Ω·m, and no constraints were applied in terms of structural or conductivity features. The error floor used for the inversion was 5% for the impedance tensor, and the misfit between the observed data and the final model responses has an RMS value of 1.95.

Fig. 3 compares the observed data and the model responses as pseudosections, showing that major features in the data are explained by the model. Data fit is shown in Fig. S1 (supplementary material) as apparent resistivity and phase curves for each site used in the inversion. The resulting final model, which will be discussed in the following sections, is shown in Fig. 4. The Figure also includes the geological map and the description of the well Tamurcia-1 for reference (Lanaja, 1987; see Fig. 1 for location).

2.2. Gravity data

Gravimetry is a commonly used method to investigate variations in the distribution of rock density within the Earth's crust. In the study area, a total of 2449 data points from the Institut Cartogràfic i Geològic de Catalunya (ICGC) database were integrated with 1141 new stations acquired and processed to create a detailed Bouguer anomaly map of the Central Pyrenees. The point distribution of the data is approximately 1 point per square kilometre (Ayala et al., 2021). The new gravity data were collected using three different gravimeters with varying levels of accuracy: Scintrex CG5 (accuracy of 0.001 mGal), Lacoste & Romberg G582 (accuracy of 0.005 mGal), and Scintrex CG6 (accuracy of 0.001 mGal). The station location (i.e., horizontal coordinates (X, Y) and elevation (Z)) was measured using a differential GNSS instrument (JAVAD's TRIUMPH) which has centimetre accuracy. Further details on the data processing can be found in Ayala et al. (2021).

The Bouguer anomaly map of the study area exhibits a long-wavelength elongated minimum of approximately 100.0 mGal, which extends towards the east and west. This minimum can be associated with crustal thickening in the Pyrenean root (Fig. 5) (e.g., Torné et al., 2015). The gradients towards the north and south indicate crustal thinning in those directions. The map also reveals various relative maxima and minima of medium and short wavelengths with variable amplitudes, which could be associated with shallower structures. Two notable features are observed on the map. Firstly, the La Maladeta granite is characterized by lateral variations in the Bouguer anomaly ranging from −100 to −90 mGal. The most prominent feature is a minimum located in its central part, which extends to the north and encompasses the outcrop of a smaller granite known as the Arties granite. The second important feature is a relative minimum (amplitudes up to c. 20 mGal), which is located to the SW of the La Maladeta granite. This feature is interpreted as the gravimetric response to Triassic evaporitic layers, which are apparently far larger than the mapped outcrops (Clariana et al., 2022; Soto et al., 2022).

Since we focus on the upper crust, for this work we have modelled the residual Bouguer anomaly that was obtained by subtracting a third-degree polynomial regional anomaly from the Bouguer anomaly. This residual Bouguer anomaly reflects the contribution of the sources at a depth of up to 10 km (Ayala et al., 2021).

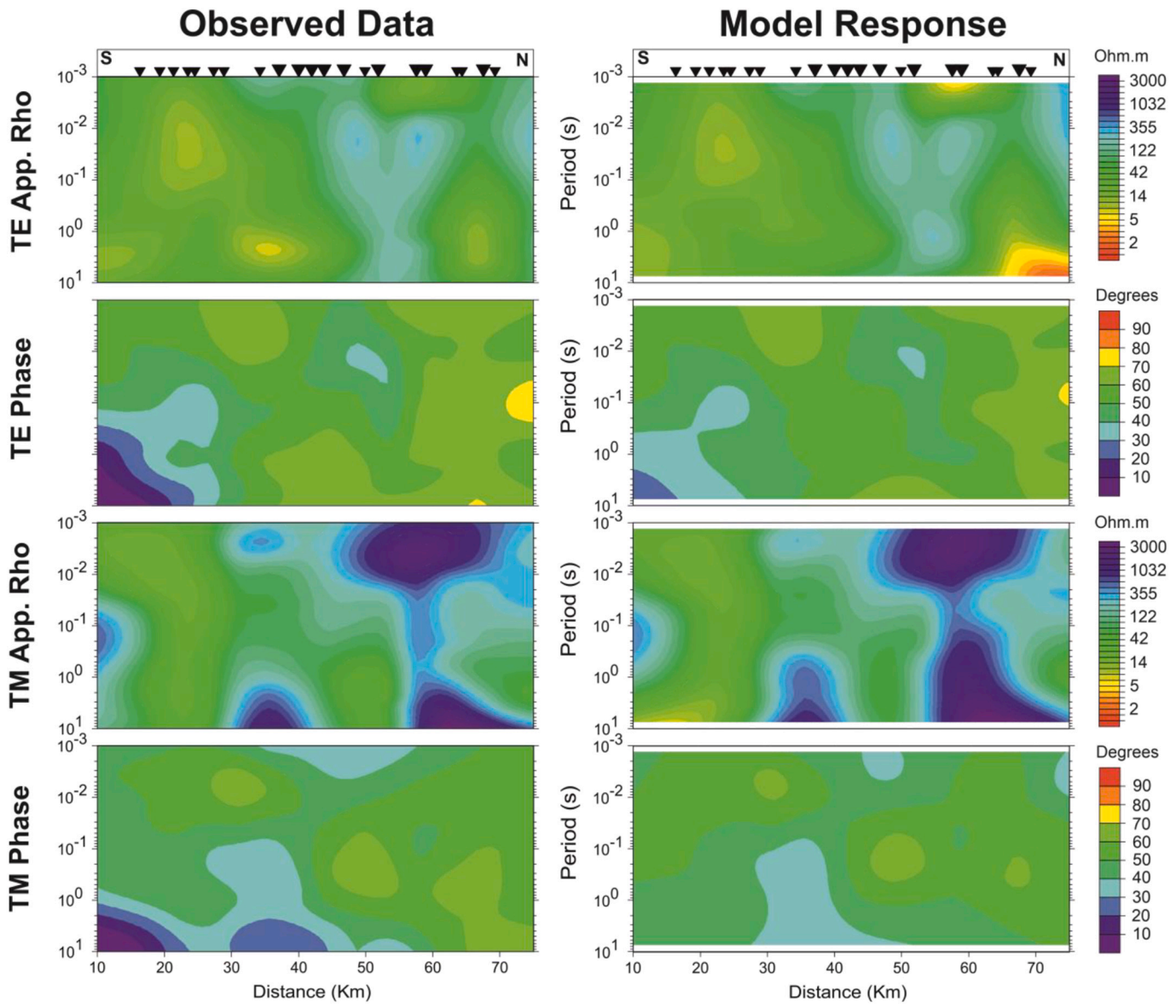

Fig. 3. Comparison of apparent resistivity and phases of TM and TE mode for the observed data and model responses.

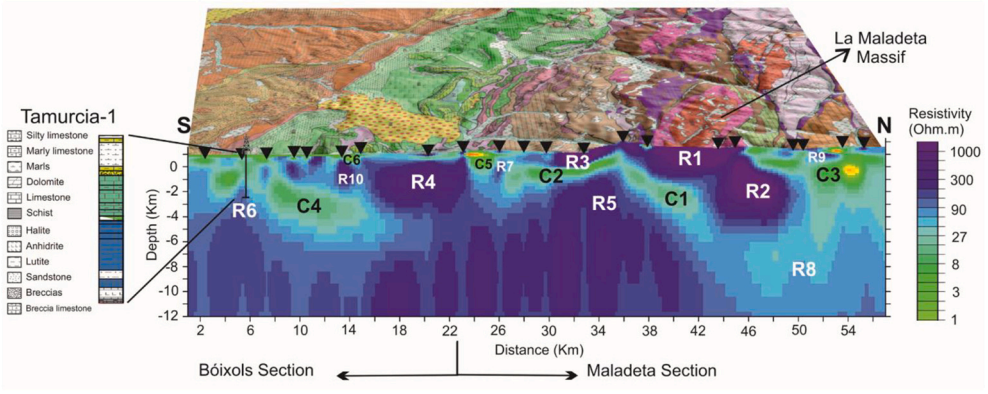

Fig. 4. Two-dimensional MT resistivity model obtained by inversion using both TE and TM mode resistivity and phases, together with the mapped geology (See Fig. 1b for geological legend) and the information provided by the Tamurcia-1 well. The main geoelectrical features are labelled "R" for high-resistivity structures and "C" for low resistivity structures (See text for more information).

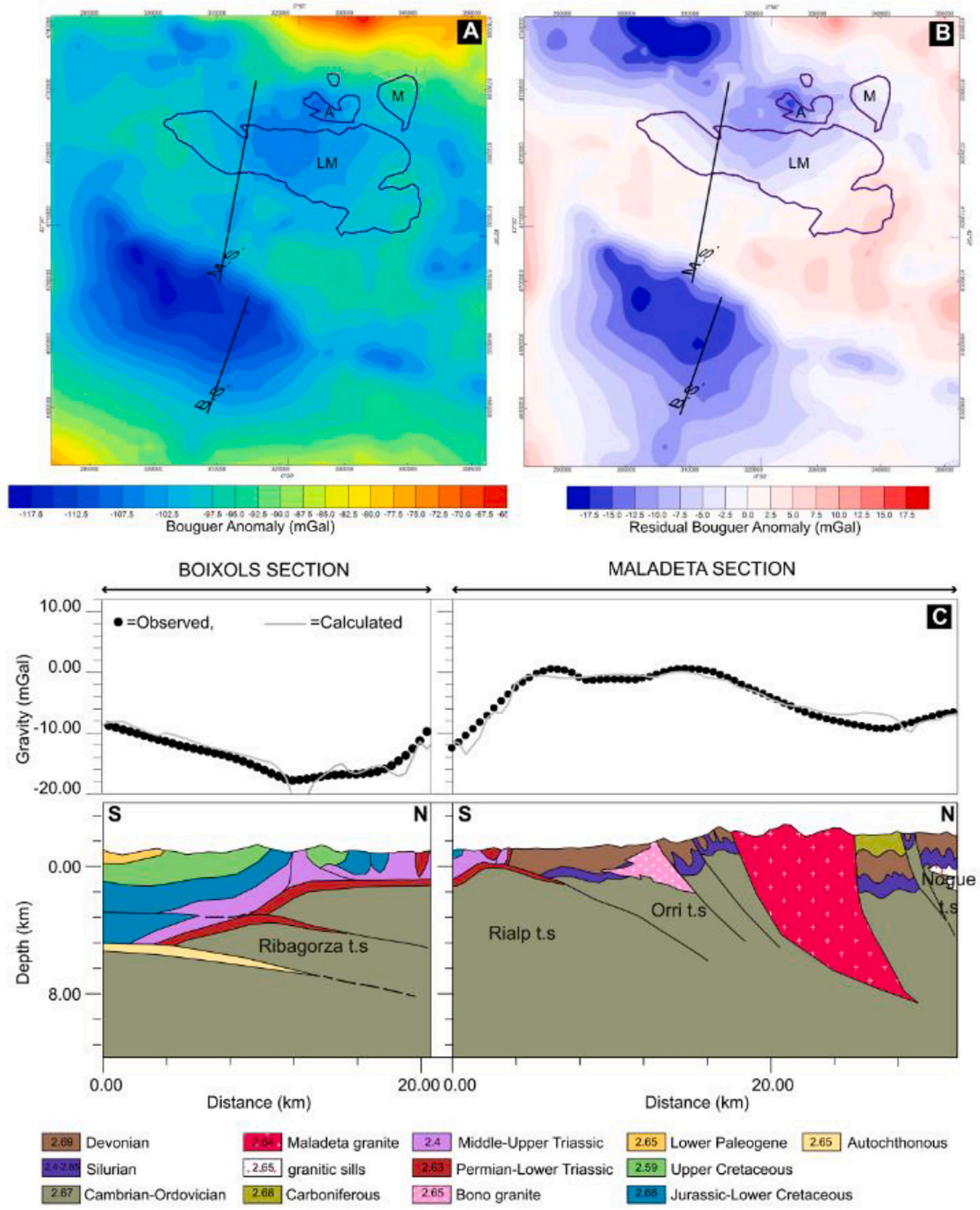

Fig. 5. a) Bouguer anomaly of the study area. B) Residual Bouguer anomaly of the study area. Straight black line: Location of the gravimetric profiles (BS: Boixols section; MS: Maladeta section); Black lines: Outline of the granites (LM: La Maladeta batholith; A: Arties granite). UTM coordinates in m, zone 31, ETRS89 datum. c) Gravimetric profile modelled before integrating the results of the MT interpretation. Density values for each unit are in g/cm^3.

In the residual Bouguer anomaly map (Fig. 5), the La Maladeta batholith exhibits a gravimetric zonation that may reflect internal lateral compositional changes (Clariana et al., 2022). This zonation is characterized by small variations in amplitude, ranging from −10 to 6 mGal. The Arties granite, which is a smaller granite located within the La Maladeta batholith, shows a smaller anomaly but still reaches negative values ranging between −12 and − 4 mGal. To the south of the La Maladeta batholith, the gravity minimum observed in the Bouguer anomaly map becomes even more prominent, with values ranging from −18 to −4 mGal.

3. Results

MT and gravity models cross two clearly differentiated geological domains: the Axial Zone in the northern part, where significant granitic bodies outcrop (such as the La Maladeta granite), and the South-Central-

Pyrenean zone in the southern area, characterized by the Bóixols thrust sheet. Consequently, the presentation of results and subsequent discussion will be conducted separately for these two sections.

3.1. MT inversion: 2-D resistivity model

Fig. 4 shows the final 2-D resistivity model, where the most striking geoelectrical features are labelled "R" for high-resistivity structures and "C" for low resistivity ones. In this section, we provide a general description and preliminary interpretation of the main features, while a more comprehensive geological analysis will be presented in the discussion section.

In the La Maladeta section there are several outstanding features. Features **R1 and R2** are located on the northern part of the model where they show the highest resistivity values, up to 4000 Ω·m. These values are observed from the shallowest areas of the model to depths of ~3 km below sea level (b.s.l) and correspond to the outcropping granites of the La Maladeta massif, characterized by Ortuño et al. (2008) as highly resistive. In between these two bodies there is a small zone with lower resistivity values (< 1000 Ω·m). To ascertain the resolution of the MT data against this low-resistivity zone, we performed a non-linear-sensitivity test (e.g., Ledo and Jones, 2005; Piña-Varas et al., 2018). By comparing the MT responses of the final (Fig. 4) and modified models (Fig. S2 in the supplementary material), we can determine the effect on the data fit of removing this low-resistivity zone. The result shows that, while considering only one single high-resistivity body, it leads to a significant increase in the data misfit. As a result, structures R1 and R2 must be examined as two independent high-resistivity bodies separated by a lower resistivity zone.

The structure **R3** is similar to the R1 and R2 features in terms of resistivity values but with a significantly shallower depth extent. This feature is also observed from the shallower zones of the model and coincides with the location of the outcrop of the Bono granodiorites and metamorphic rocks. **C1 and C2** are located below the high-resistivity features described above. The area below R3, the body labelled C2, is characterized by resistivity values lower than 20 Ω·m with a moderately southward dipping trend. In contrast, the structure located underneath R1 and R2 (C1) shows a clear and strong northward dipping tendency and slightly higher resistivity values (> 50 Ω·m). In this case the preliminary interpretation indicates that a structural feature (e.g., the fault zone) is present. These two geoelectrical features were validated by performing a sensitivity test, similar to what has been explained above for features R1 and R2 (Fig. S3 in the supplementary material).

There are **other minor features** worth mentioning. The northern and southernmost parts of the profile are characterized by overall low resistivity values (< 10 Ω·m), which correlate to the Aran Valley's Devonian fill units and the Nogueras Zone, labelled **C3 and C5**, respectively). Some resistive bodies are also observed in this area, such as **R7** with resistivity values higher than 150 Ω·m and a pronounced subvertical geometry, in addition to **R9,** with slightly higher resistivity values (around 250 Ω·m).

In the Bóixols section, the model shows three major geoelectrical features. The high-resistivity body labelled **R4** is consistent with the location of a thick succession of carbonates (marls, limestones, and dolomites) and evaporites. Both the northern and southern limits of this structure show much lower resistivity values (**C5** and **C6**), which correspond to the outcropping Upper Triassic units (salt, anhydrite, and mudstones). The southernmost part of the profile is characterized by low resistivity values (**C4**), even though in this area the mapped geology also shows carbonate units similar to those located around the R4 feature. Other geoelectrical features resolved in this area are **R6** and **R10**.

Finally, a high-resistivity structure labelled **R5** could be interpreted as the Pre-Variscan basement, which seems to reach its shallowest depths in the central part of the profile.

3.2. Gravity data modelling

3.2.1. Geological cross-section

The first step in constructing the gravity-constrained model was to develop a geological cross-section based on previous data. This geological section is oriented perpendicular to the main structures (Fig. 1b), overlapping with the MT model in its central and northern part (La Maladeta section). However, there is a slight discrepancy in the trace of the MT and gravity models to the south (Bóixols section), since the MT dataset in this area was collected in a previous survey (as explained above) (Figs. 1b and 2).

Data from several geological maps were used to build the framework of the entire geological profile (Rosell, 1994; Ríos-Aragües et al., 2002; García-Senz and Ramirez-Merino, 2009; García-Sansegundo and Ramírez Merino, 2013; López-Olmedo and Ardèvol, 2016; ICGC, 2016). The subsurface structure of the southern part of the profile (i.e., Bóixols thrust sheet) has been previously interpreted based on well and seismic data (Teixell and Muñoz, 2000; García-Senz, 2002; Mencos et al., 2015; Saura et al., 2016; Muñoz et al., 2018). This profile also benefits from two close and parallel gravity-constrained cross-sections that have been recently published (Clariana et al., 2022). The proximity of our geological profile to the oil exploration well Cajigar-1 (Lanaja, 1987) has allowed us to delineate the position of the Upper Triassic evaporites at depth and to determine the thickness of the Jurassic limestones (Fig. 5). The minimum depth to the top of the basement was calculated based on data obtained from the Comiols-1 and Isona-1 wells (Teixell and Muñoz, 2000) (Fig. 5). The northern section of the profile crosses the Axial Zone, where the only subsurface data available are derived from the ECORS-Pyrenees deep seismic reflection profile (e.g., Choukroune et al., 1989). In this part of the profile, we have compiled previously published structural interpretations (Poblet, 1991; García-Sansegundo, 1992; Gutiérrez-Medina, 2007; Izquierdo-Llavall et al., 2013).

The geological cross section shows a distinctive northern and southern half, but with a common southward vergence of most of the structures (Fig. 5). The northern part corresponds to the Axial Zone, composed of Palaeozoic rocks and characterized by northward-dipping thrusts with moderate to steep dips that cut across and/or reactivate previous Variscan structures (Gil-Peña, 2004; Cochelín et al., 2017a). The southern part corresponds to the South Pyrenean Zone, which is characterized by the presence of a Mesozoic-Cenozoic cover that is detached from the basement along a décollement formed by the Upper Triassic evaporites. In the Axial Zone, from north to south, the profile crosses the following outcropping alpine basement thrust sheets described by Muñoz (1992): the Nogueras and Orri thrust sheets and the Nogueras Zone. The northernmost unit, the Nogueras thrust sheet (Gavarnie unit according to Waldner et al., 2021), consists of Silurian and Devonian slates and limestones (García-Sansegundo and Ramírez-Merino, 2013). To the south, the Orri thrust sheet consists of highly deformed Cambro-Ordovician slates and quartzites, Silurian shales, Devonian slates, and limestones (Gutiérrez-Medina, 2007; Izquierdo-Llavall et al., 2013) as well as Lower Carboniferous rocks together with two Late Carboniferous intrusions, the Bono and La Maladeta granites (Fig. 1b). The southernmost unit of the Axial Zone that is crossed by the profile consists of a downward facing anticline involving Lower Triassic red beds belonging to the Nogueras Zone (Seguret, 1972).

In the South Pyrenean Zone, the profile only crosses the Bóixols thrust sheet at the surface. Below the décollement (i.e., Upper Triassic evaporites), we interpret the presence of two hidden basement thrust sheets, the Rialp and Ribagorza thrust sheets from north to south, following Teixell and Muñoz (2000), Muñoz et al. (2018), and Clariana et al. (2022) (Fig. 5). The Mesozoic-Cenozoic cover that forms the Bóixols thrust sheet shows a thickness increase towards the south. This feature matches with the interpretation of Teixell and Muñoz (2000) and García-Senz (2002), who consider the Bóixols thrust sheet to be an asymmetric inverted Mesozoic basin. The Jurassic sequence is duplicated due to the southward-directed Bóixols thrust (Teixell and Muñoz,

2000; Muñoz et al., 2018). This profile is characterized by a thick layer of Upper Triassic evaporites at the base and in the Nogueras Zone. In the southern part of the cross-section Cenozoic rocks lie unconformably above the Mesozoic succession (Fig. 5).

3.2.2. 2-D gravity model

The initial geological cross-section was further constrained through an iterative feedback process between the geological information and the gravity model. This feedback ended when the calculated gravity response corresponded to the observed gravity. The final RMS of the difference between the observed and calculated anomaly is 1.121 mGal.

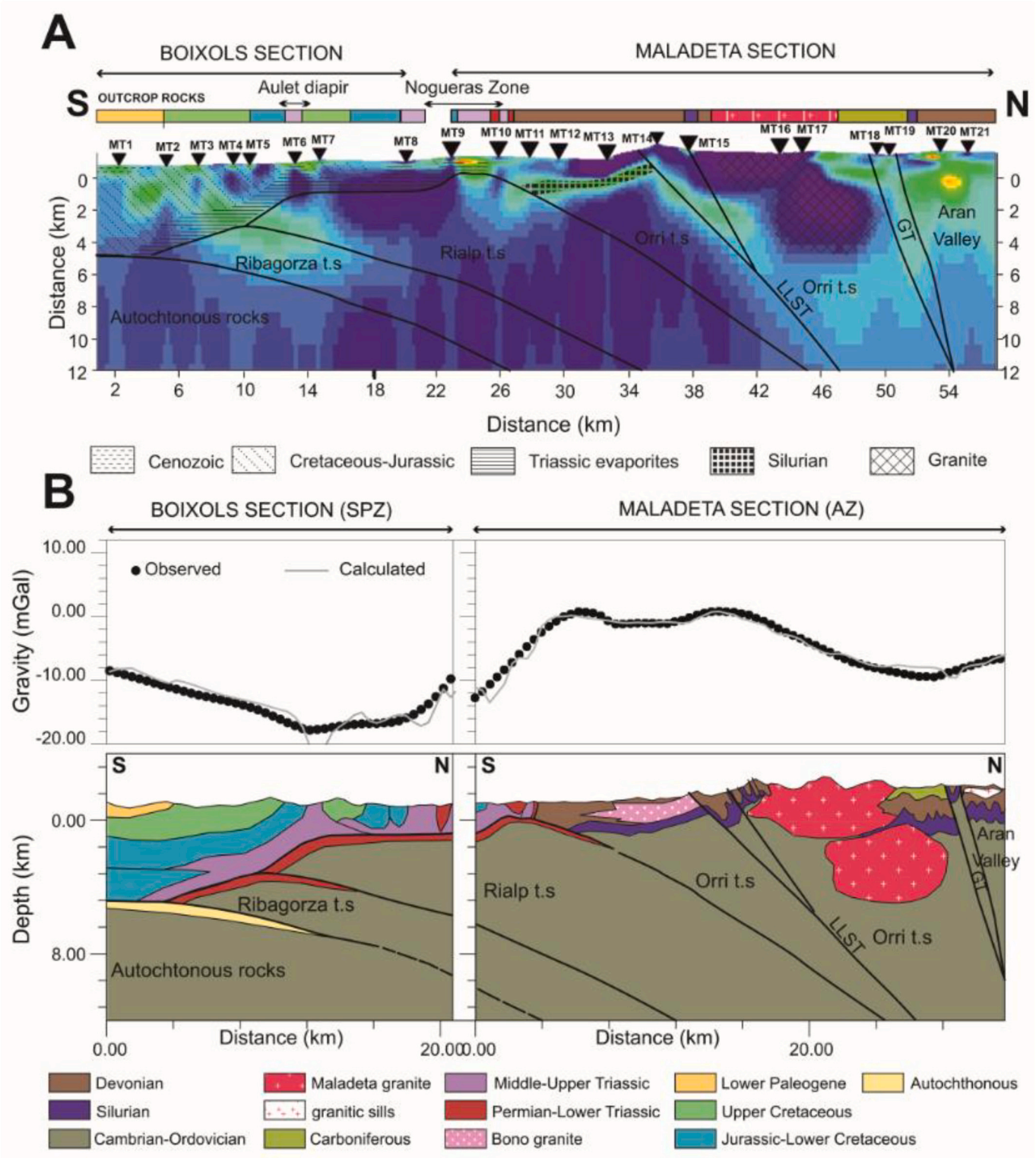

Fig. 6. Integration of results. a) MT model with the major faults and thrusts interpreted (continuous black lines) and the basement thrust sheet (e.g. Orri t.s). b) Final interpretation of the geometry at depth of the Bóixols and La Maladeta sections showing its final observed and calculated gravity data. AZ: Axial Zone; SPZ: South Pyrenean Zone; LLST: Llavorsí-Senet thrust; GT: Gavarnie thrust.

The modelling was carried out using the GM-SYS module of the Oasis Montaj® software by Geosoft based on the Talwani et al. (1959) and Won and Bevis (1987) algorithms. The profile was extended just far enough to avoid edge effects. Since the target was the upper crust, we used the residual Bouguer anomaly as the observable reflecting the contribution of sources at depths of up to 10 km (Ayala et al., 2021).

The observed gravity curve along the profile (Fig. 5C) shows two clearly differentiated parts: the northern part coinciding with the Axial Zone and the southern part with the South Pyrenean Zone (i.e., the Bóixols thrust sheet). Together the observed gravity curve exhibits a steep decrease coinciding with the Nogueras Zone and its continuation southwards. The observed gravity curve coinciding with the Axial Zone is characterized by a relatively long gravity maximum (0.5 mGal) with an approximately flat geometry that decreases towards the north, reaching a relative gravity minimum (−10 mGal). The gravity maximum coincides at the surface with highly deformed Devonian and Silurian rocks. At its central part, it shows a small relative minimum with positive values coinciding with the small outcrop of the Bono granite, thus being compatible with the presence of higher volumes of granite at depth. Towards the north, the observed gravity curve begins to decrease, coinciding with the southern end of the La Maladeta granite, and reaching its minimum value a few kilometres north of its northern end. The gravity data are compatible with an asymmetric granitic body, which is up to 8.5 km thicker in its northern sector (Fig. 5C).

In the South Pyrenean Zone (i.e., Bóixols thrust sheet), the observed gravity curve shows a prominent relative gravity minimum (−17 mGal) coinciding with the northern end of the Bóixols thrust sheet and with the front at the depth of the Rialp basement thrust sheet (Fig. 6). The lowest values of this wide negative anomaly are found just south of an outcropping diapir (the so-called Pont de Suert diapir), so this gravity low may be consistent with a significant accumulation of Triassic evaporites in the subsurface. Towards the south, the observed gravity curve increases in accordance with an increase in the thickness of the Mesozoic-Cenozoic cover and a decrease in the thickness of the Triassic evaporites at depth. In the southern part of the profile, the autochthonous materials are located at a depth of approximately 5 km, coinciding with values observed in nearby geological cross-sections constructed by Teixell and Muñoz (2000); Muñoz et al. (2018); and Clariana et al. (2022).

4. Discussion

As with the results section, here we describe the joint interpretation of both geophysical models separately for each of the two major geological zones: La Maladeta and the Bóixols sections.

Fig. 6 shows the final interpreted geological sections integrating both techniques: the MT and gravity data, together with previous geological information and the resulting calculated gravity curve across them. The RMS of the final model is 0.996 mGal.

4.1. Northern sector: La Maladeta section

In the northern section (right hand side in Fig. 6), there is a good agreement between the gravity and MT models, providing significant and novel information about the **La Maladeta granite** and the main structures at depth. A quick examination of both MT (Fig. 4) and gravity (Fig. 5) models shows that the La Maladeta granitic body exhibits high resistivity and low density values, with a clear northward dip. The most notable feature observed in the resistivity model is the presence of two distinct units within the La Maladeta granite, separated by a lower resistivity area. The validity of this low resistivity area has been confirmed through various sensitivity tests (see Section 3.1 and Fig. S2 in the supplementary material). The decrease in resistivity could be attributed to the existence of either a tectonic feature, such as a fault, or two independent granitic bodies. Interpreting this resistivity discontinuity as due to a fault (e.g., a back thrust) contradicts the known geology of the area, as no major southward dipping structures of such magnitude have been observed in this section of the Axial Zone (García-Sansegundo, 1992), nor a few kilometres to the east in the ECORS profile cross-section (Muñoz, 1992; Teixell et al., 2018). The second possible explanation for this resistivity discontinuity relates to the presence of granites associated with at least two distinct intrusive pulses. This hypothesis is plausible due to the complex nature of the La Maladeta massif, which has been interpreted as a combination of multiple plutons based on geological, geochemical, and magnetic fabric data collected at the surface (Michard-Vitrac et al., 1980; Leblanc et al., 1994). Considering the large time span (50 Ma) over which Late Variscan plutons in the Axial Zone had been emplaced (Bouchez and Gleizes, 1995; Evans et al., 1998; Gleizes et al., 2001), the presence of multiple intrusive events is feasible. The La Maladeta granite, interpreted as the shallow body in our MT profile, was emplaced around 298 ± 2 Ma (Evans, 1993; Solé et al., 1997; Esteban et al., 2015). This age is younger than the most common crystallization age observed in the large Variscan granites of the Axial Zone (310–300 Ma), but is older than other Early Permian granites and granodiorites dated between 298 and 290 Ma in the Axial Zone (López-Sánchez et al., 2019; Schnapperelle et al., 2020). Our data do not allow for the determination of the relative chronology of the two granitic bodies observed in the MT profile. Both possibilities (the deeper granite being younger or older compared to the shallow one) are plausible, considering the characteristics of Late Variscan magmatism in the Axial Zone. Further studies would be required to ascertain the relative timing.

Another significant result of our study is the depth extension of the La Maladeta massif, which reaches nearly 8 km in this section. This implies a greater depth than previous interpretations (Muñoz et al., 2018) (Fig. 8). The depth may be even greater towards the east, where the La Maladeta massif exhibits a broader north-south longitudinal extension. The substantial size of this granitic body relative to the surrounding metasediments suggests an important rheological inheritance that could influence the width of the Alpine Orri thrust sheet.

Recently, Waldner et al. (2021) interpreted the La Maladeta granite as a single body with its base located approximately 20 km below the pre-shortening stage (84 Ma) based on thermochronological and previously published data. This depth corresponds with the possible base of the deeper granite identified in the present study. Considering the MT model, the geometry of the La Maladeta massif at depth exhibits only slight differences compared to the gravity-constrained section (Fig. 5). In the resistivity model, this granitic massif is less inclined towards the north and reaches a shallower depth (Fig. 6). The higher resistivity area characterizing the La Maladeta granite outcrop continues southward at depth (Fig. 4), suggesting the presence of granite beneath a highly deformed region comprising Silurian and Devonian rocks. Additionally, considering the gravity response in this area, which displays a relative gravity maximum (Fig. 5), we also interpret the presence of rocks affected by contact metamorphism. The granitic massif is delimited to the north and south by low resistivity zones (labelled C1 and C3 in Fig. 4), which could be associated with major thrusts involved in the antiformal geometry of the Axial Zone (Llavorsí-Senet and Gavarnie alpine thrusts; Fig. 6). These structures exhibit a steep dip to the north and are influenced by the presence of Silurian shales in the area. The significant role of Silurian shales as a detachment level in the Axial Zone, during both the Variscan and Alpine Orogenies, has been previously described by several authors (Matte, 1969; García-Sansegundo, 1990; García-Sansegundo et al., 2011; Marcén et al., 2018; Cochelin et al., 2017a; Casas et al., 2019).

Similar to La Maladeta, **the Bono granite** is characterized by high resistivity values (R3 in Fig. 4) and has a narrow outcropping area. However, its geometry at depth, as interpreted from the MT data, differs from that inferred from the gravity data. The MT data suggests a laminar geometry for the Bono granite, indicating a relatively shallow depth. Nearby granites, such as the Marimanha granite (Antolin et al., 2009) and other Pyrenean granites (Olivier et al., 1999; Gleizes et al., 2001), have been interpreted to exhibit laccolite geometry based on magnetic

and structural data. This type of geometry may result from upward and lateral expansion of magma along rheological boundaries, similar to those existing between the siliciclastic Cambro-Ordovician rocks and the Silurian-Devonian limestone and shales. The root of the Bono granite appears to be influenced by the Bono thrust. The resistivity model reveals a conductive feature beneath the Bono granite (labelled as Feature C2 in Fig. 4), which may be associated with Silurian units, such as shales, that are present in the area (Fig. 6). As mentioned previously, the Silurian rocks represent a regional detachment level (e.g., García-Sansegundo et al., 2011), which could have also facilitated the emplacement of granites during the Late Carboniferous-Permian period.

The southern region of the Axial Zone, specifically the southern Orri basement thrust sheet (Fig. 6), exhibits a relative gravity maximum that corresponds to extensive outcrops of highly deformed Devonian units, as well as Devonian, Silurian, and Cambro-Ordovician rocks at depth. In this area, the resistivity model reveals a nearly vertical high resistivity feature (labelled as R7 in Fig. 4), which correlates with the interpreted vertical beds of Lower Triassic rocks (Fig. 6). Additionally, a shallow conductive feature (labelled as C5 in Fig. 4) is observed in the resistivity model, which could be associated with downward thrusts linked to the Nogueras Zone. These features align well with the geometry inferred from the gravity-constrained section.

Finally, the **Aran Valley sinclinorium**, situated in the northernmost part of this section, is characterized by a series of folded and faulted Devonian-Silurian units. The abundance of highly faulted black slates and lutites (Kleinsmiede, 1960; García-Sansegundo, 1992; García-Sansegundo et al., 2013; Cochelin et al., 2017) may contribute to an overall low electrical resistivity. However, higher resistivity values are also observed, such as the feature labelled as R9 in Fig. 4, which may be associated with small and shallow granite bodies previously interpreted in the gravity-constrained section as being related to the **Artiés granite**.

At depth, the Orri basement thrust sheet exhibits a high resistivity pre-Variscan basement, which is characterized by an abrupt resistivity change towards the north (Fig. 6). This change may be attributed to the involvement of different units within the various basement thrust sheets, highlighting the significance of structures such as the Llavorsí-Senet thrust sheet as major boundaries separating distinct resistivity units likely associated with varying metamorphic conditions. Therefore, in the context of the Pyrenean Axial Zone, areas of low electrical resistivity could be linked to the presence of Silurian shales and/or major faults, which facilitate fluid migration, while regions of high electrical resistivity primarily correspond to granite bodies. Notably, the MT data provides higher resolution compared to gravity-constrained sections for inferring the deep geometry of granitic bodies and tracing the major alpine faults at depth. The thrust dips that are observed in this section across the Axial Zone have been interpreted to exhibit similar angles and therefore imply the same amount of shortening as proposed in previous studies (e.g., Muñoz, 1992; Muñoz et al., 2018). This interpretation is based on the limited resolution of the two geophysical techniques to precisely determine the dip of structures.

4.2. Southern sector: Bóixols section

This region is characterized by the presence of thick Mesozoic sedimentary successions, primarily carbonates, which are detached from the basement along the Triassic evaporites (Keuper). Extensive outcrops of Triassic evaporites are found in certain areas of the South Pyrenean Zone, while along the profile **Triassic units** are observed in limited selected areas. One notable example is the Aulet diapir, where we observe a strong agreement between the gravity data (Figs. 5 and 6) and the resistivity model (labelled as C6-R6 in Fig. 4). These diapirs exhibit low electrical resistivity at shallow depths and density values ranging from 2.4 g/cm^3 (Middle-Upper Triassic) to 2.63 g/cm^3 (Lower Triassic). At greater depths, the resistivity pattern transitions to higher resistivity values, likely attributable to variations in water content within these units from shallow to deeper areas (Rubinat et al., 2010).

In the MT model, we observe moderate to high resistivity values in the southern edge of the profile from approximately 2 km below the surface (labelled as R6 in Fig. 4). These values may be associated with the accumulation of Triassic evaporitic rocks at depth, possibly related to the leading edges of the Rialp and Ribagorza basement thrust sheets (Fig. 6). This interpretation is supported by the information obtained from the Tamurcia-1 well, where its lower portion is dominated by the presence of salts (Fig. 4).

Jurassic and Cretaceous units are characterized by thick successions that are primarily composed of marls, limestones, and dolomites. These units display a similar response in the gravity data, with density values ranging from approximately 2.65 to 2.675 g/cm^3. However, the MT responses are strongly influenced by the rock type (limestone, dolomite, etc.), the presence of marls and water, and the occurrence of faults. As a result, these units may exhibit a wider range of electrical resistivity values. This would explain the observed resistivity contrast between the northern and southern parts of this section, despite the absence of major lithological changes in the gravity model.

The information derived from the Tamurcia-1 well (Lanaja, 1987; see Fig. 1 for location) indicates that the upper part of the well, comprising Upper Cretaceous rocks, primarily consists of alternating layers of marls and silty limestones, which are characterized by low resistivity values in our resistivity model. These low resistivity values are also detected in the north in the feature labelled as C6, corresponding to Upper Cretaceous rocks (Fig. 6). Lower Cretaceous units are relatively sparse in this well, as in the south-central Pyrenees, exhibiting significant thickness variations ranging from a few meters to up to 4000 m (e.g., Berástegui et al., 1990; García-Senz, 2002; Mencos et al., 2015). Therefore, the lower portion of the well primarily corresponds to Jurassic units, predominantly composed of dolomites. The MT model reveals a slight increase in electrical resistivity in the lower part of this area, showing a high correlation with the information provided by the well log. To the north of the well, the structure becomes more complex, featuring a series of faults and folds that affect the entire sequence, including the Lower Cretaceous rocks located at the core of these folds.

In the northern part of this section, the high resistivity structure (labelled as R4 in Fig. 4) resolved by the MT model corresponds to significant accumulations of Triassic evaporites and thick folded packages of Jurassic and Cretaceous limestones above 1000 m depth, along with the upper part of the Rialp basement thrust sheet 1000 m depth. The low resistivity feature labelled as C4 may correspond to the Rialp thrust (Fig. 6). In general, the MT model exhibits a complex resistivity pattern (Figs. 4 and 6) in the Bóixols section due to the presence of Mesozoic rocks with varying lithologies (such as limestones, marls, and evaporites) and variations in water content and deformation gradient (including faults and folds). On the other hand, the gravity model appears to be heavily influenced by the presence of low-density rocks (such as Triassic evaporites) at depth (Figs. 4 and 6).

5. Conclusions

The integration of MT and gravity data has provided valuable and novel insights into the geological structure at the boundary between the Axial Zone and the South Pyrenean Zone, specifically through the La Maladeta batholith. The joint interpretation of both geophysical models, in conjunction with existing geological information, has played a crucial role in the final geological interpretation.

The geometry of the La Maladeta massif at depth has been successfully resolved by both the gravity and resistivity models, displaying good agreement. This study has revealed a noteworthy aspect of the massif: it consists of two distinct granitic bodies at depth, likely associated with different intrusive pulses, while reaching a greater depth than previously interpreted. This newfound information has significant implications for comprehending the geological evolution of the study area.

Furthermore, the structure of the northern boundary of the South-Central Pyrenean Zone in the proximity of the Tamurcia-1 well

(Bòixols section) has been resolved, unveiling a series of faults and folds that affect the entire sequence. This geological understanding allows for the identification of areas where Triassic units are exposed along the profile.

CRediT authorship contribution statement

P. Piña-Varas: Writing – review & editing, Writing – original draft, Visualization, Resources, Methodology, Investigation, Conceptualization. **R. Soto:** Writing – review & editing, Writing – original draft, Validation, Conceptualization. **P. Clariana:** Writing – review & editing, Writing – original draft, Validation, Conceptualization. **C. Ayala:** Project administration, Methodology, Funding acquisition, Conceptualization. **F. Rubio:** Validation, Supervision, Resources, Conceptualization. **J. Ledo:** Validation, Supervision, Conceptualization. **C. Rey-Moral:** Resources, Conceptualization. **A. Martí:** Conceptualization, Validation. **G. Mitjanas:** Data curation. **P. Queralt:** Validation, Conceptualization. **A. Marcuello:** Validation, Conceptualization. **P. Santolaria:** Validation, Conceptualization. **E. Pueyo:** Validation, Conceptualization.

Declaration of Competing Interest

The authors declare that they have no known competing financial interests or personal relationships that could have appeared to influence the work reported in this paper.

Data availability

Data will be made available on request.

Acknowledgments

This work was funded by projects PID2020-114273GB-C22 and PID2020-113135RB-C31 funded by MCIN/AEI/10.13039/501100011033 and CGL2017-82169-C2-2-R, from the Spanish Ministry of Science and Innovation. The authors acknowledge the contribution of José María Llorente, Agustín González, and Arturo García for the acquisition of the gravity data. This study also represents a contribution to GeoAp Research Group (E01-20R) (Aragón Government).

We express our sincere gratitude to the editor and reviewers for their valuable time and efforts in reviewing our manuscript. Their critical feedback has greatly contributed to the improvement of our work.

Appendix A. Supplementary data

Supplementary data to this article can be found online at https://doi.org/10.1016/j.tecto.2023.230022.

References

Ayala, C., Rey-Moral, C., Rubio, F., Soto, R., Clariana, P., Martín-León, J., Bellmunt, F., Gabàs, A., Macau, A., Casas, A.M., Martí, J., Pueyo, E.L., Benjumea, B., 2021. Gravity data on the Central Pyrenees: a step forward to help a better understanding of the Pyrenean structures. J. Maps. https://doi.org/10.1080/17445647.2021.2001386.

Ayala, C., Benjumea, B., Mediato, J.F., García-Crespo, J., Clariana, P., Soto, R., Rubio, F., Rey-Moral, C., Pueyo, E.L., Martín-León, J., García, A.G., Fernández-Canteli, P., Martínez-Orio, R., 2022. Developing a new innovative methodology to integrate geophysical techniques into characterization of potential CO2 storage sites: Lopín structure (Southern Ebro basin, Spain). Geol. Soc. Lond., Spec. Publ. 528 (1). SP528-2022.

Barnolas, A., Chiron, J.C., 1996. Synthèse Géologique et Géophysique des Pyréenées, Volume 1: Introduction. Géophysique. Cycle Hercynien, ed. BRGM-ITGE, Orléans, France, p. 729.

Beaumont, C., Muñoz, J.A., Hamilton, J., Fullsack, P., 2000. Factors controlling the Alpine evolution of central Pyrenees inferred from a comparison of observations and geodynamical models. J. Geophys. Res. Solid Earth 105 (B4), 8121–8145. https://doi.org/10.1029/1999JB900390.

Bouchez, J.L., Gleizes, G., 1995. Two-stage deformation of the Mont-Louis-Andorra granite pluton (Variscan Pyrenees) inferred from magnetic susceptibility anisotropy. J. Geol. Soc. 152, 669–679. Retrieved from. https://api.semanticscholar.org/CorpusID:129911398.

Burrel, L., Teixell, A., Gómez-Gras, D., Coll, X., 2021. Basement-involved thrusting, salt migration and intramontane conglomerates: a case from the Southern Pyrenees. Bull. Soc. Géol. Fr. – Earth Sci. Bull. 191 https://doi.org/10.1051/bsgf/2021013.

Campanyà, J., Ledo, J., Queralt, P., Marcuello, A., Liesa, M., Muñoz, J.A., 2011. Lithospheric characterization of the Central Pyrenees based on new magnetotelluric data. Terra Nova 23 (3), 213–219.

Campanyà, J., Ledo, J., Queralt, P., Marcuello, A., Liesa, M., Muñoz, J.A., 2012. New geoelectrical characterisation of a continental collision zone in the West-Central Pyrenees: constraints from long period and broadband magnetotellurics. Earth Planet. Sci. Lett. 333, 112–121.

Casas, J.M., Clariana, P., García-Sansegundo, J., Margalef, A., Puddu, C., Sanz-López, J., et al., 2019. The Pyrenees. In: Quesada, C., Oliveira, J. (Eds.), The Geology of Iberia: A Geodynamic Approach. Regional Geology Reviews. Springer. https://doi.org/10.1007/978-3-030-10519-8_8, pp. 335–259.

Chevrot, S., Villaseñor, A., Sylvander, M., Benahmed, S., Beucler, E., Cougoulat, G., et al., 2014. High-resolution imaging of the Pyrenees and Massif Central from the data of the PYROPE and IBERARRAY portable array deployments. J. Geophys. Res. Solid Earth 119 (8), 6399–6420. https://doi.org/10.1002/2014jb010953.

Chevrot, S., Sylvander, M., Díaz, J., Martin, R., Mouthereau, F., Manatschal, G., Ruiz, M., 2018. The non-cylindrical crustal architecture of the Pyrenees. Sci. Rep. 8 (1), 9591.

Chevrot, S., Sylvander, M., Villaseñor, A., Díaz, J., Stehly, L., Boué, P., Vidal, O., 2022. Passive imaging of collisional orogens: a review of a decade of geophysical studies in the PyrénéesImagerie passive des orogènes collisionnels: une revue d'une décennie d'études géophysiques dans les Pyrénées. Bull. Soc. Géol. Fr. 193 (1).

Choukroune, P., ECORS team, 1989. The ECORS Pyrenean deep seismic profile reflection data and the overall structure of an orogenic belt. Tectonics 8, 23–39. https://doi.org/10.1029/tc008i001p00023.

Clariana, P., Soto, R., Ayala, C., Casas-Sainz, A.M., Román-Berdiel, T., Oliva-Urcia, B., Pueyo, E.L., Beamud, E., Rey-Moral, C., Rubio, F., Margalef, A., Schamuells, S., Bach, N., Martí, J., 2022. Basement and cover architecture in the Central Pyrenees constrained by gravity data. Int. J. Earth Sci. https://doi.org/10.1007/s00531-021-02137-2.

Cochelin, B., Chardon, D., Denèle, Y., Gumiaux, Ch., Le Bayon, B., 2017a. Vertical strain partitioning in hot Variscan crust: syn-convergence escape of the Pyrenees in the Iberian-Armorican syntax. Bull. Soc. Géol. Fr. 188, 39. https://doi.org/10.1051/bsgf/2017206.

Cochelin, B., Lemirre, B., Denèle, Y., de Saint, B.M., Lahfd, A., Duchêne, S., 2017b. Structural inheritance in the Central Pyrenees: the Variscan to alpine tectonometamorphic evolution of the Axial Zone. J. Geol. Soc. Lond. https://doi.org/10.1144/jgs2017-066.

ECORS-Pyrenees Team, 1988. Deep reflection seismic survey across an entire orogenic belt, the ECORS Pyrenees profile. Nature 331, 508–511.

Esteban, J.J., Aranguren, A., Cuevas, J., Hilario, A., Tubia, J.M., Larionov, A., Sergeev, S., 2015. Is there a time lag between the metamorphism and emplacement of plutons in the Axial Zone of the Pyrenees? Geol. Mag. 152 (5), 935–941.

Evans, N.G., 1993. Deformation during the Emplacement of the Maladeta Granodiorite, Spanish Pyrenees. Unp. Ph.D.. University of Leeds, United Kingdom.

Evans, N.G., Gleizes, G., Leblanc, D., Bouchez, J.L., 1998. Syntectonic emplacement of the Maladeta granite (Pyrenees) deduced from relationships between Hercynian deformation and contact metamorphism. J. Geol. Soc. 155, 209–216.

Ford, M., Vergés, J., 2020. Evolution of a salt-rich transtensional rifted margin, eastern North Pyrenees, France. J. Geol. Soc. 178 (1) jgs2019-157.

Ford, M., Masini, E., Vergés, J., Pik, R., Ternois, S., Léger, J., Calassou, S., 2022. Evolution of a low convergence collisional orogen: a review of Pyrenean orogenesis. Bull. Soc. Géol. Fr. 193 (1).

García-Sansegundo, J., 1990. Structure of the Paleozoic in the Aran valley, Axial Zone, Central Pyrenees. Bull. Soc. Géol. Fr. 2, 229–239.

García-Sansegundo, J., 1992. Estratigrafía y estructura de la Zona Axial pirenaica en la transversal del Valle de Aran y de la Alta Ribagorça. Publicaciones especiales del Boletín Geológico y Minero, p. 167.

García-Sansegundo, J., Ramírez Merino, J.I., 2013. Mapa Geológico de España E. 1: 50.000, Hoja no 118bis-148 (Caneján-Viella), 2ª Serie MAGNA. Instituto Geológico y Minero de España, Madrid.

García-Sansegundo, J., Gavaldà, J., Alonso, J.L., 2004. Preuves de la discordance de l'Ordovicien supérieur dans la zona axiale de Pyrénées: example de dome de la Garonne (Espagne, France). Compt. Rendus Geosci. 336, 1035–1040.

García-Sansegundo, J., Poblet, J., Alonso, J.L., Clariana, P., 2011. Hinterland – foreland zonation of the Variscan orogen in the Central Pyrenees: comparison with the northern part of the Iberian Variscan Massif. In: Poblet, J., Lisle, R.J. (Eds.), Kinematic Evolution and Structural Styles of Fold-and-Thrust Belts. Geological Society, London, pp. 169–184. Special Publications 349.

García-Senz, J., 2002. Cuencas extensivas del Cretácico Inferior en los Pirineos centrales: formación y subsecuente inversión. PhD thesis. University of Barcelona, Barcelona, Spain, p. 310.

García-Senz, J., Ramirez-Merino, J.I., 2009. Mapa Geológico de España E. 1:50.000, Hoja no 213 (El Pont de Suert), 2ª Serie MAGNA. Instituto Geológico y Minero de España, Madrid.

García-Yeguas, A., Ledo, J., Piña-Varas, P., Prudencio, J., Queralt, P., Marcuello, A., Ibañez, J.M., Benjumea, B., Sánchez-Alzola, A., Pérez, N., 2017. A 3D joint interpretation of magnetotelluric and seismic tomographic models: the case of the volcanic island of Tenerife. Comput. Geosci. 109 (2017), 95–105.

Gil-Peña, I., 2004. Estructura alpina de la Zona Axial. In: Vera, J. (Ed.), Geología de España. SGE-IGME, Madrid, p. 241.

Gleizes, G., Leblanc, D., Olivier, P., Bouchez, J.L., 2001. Strain partitioning in a pluton during emplacement in transpressional regime: the example of the Ne'ouvielle granite (Pyrenees). Int. J. Earth Sci. 90, 325–340.

Groom, R.W., Bailey, R.C., 1989. Decomposition of magnetotelluric impedance tensors in the presence of local three-dimensional galvanic distortion. J. Geophys. Res. 94 (B2), 1913–1925.
Henke, C.H., Krieger, M.H., Strack, K., Zerilli, A., 2020. Subsalt imaging in northern Germany using multiphysics (magnetotellurics, gravity, and seismic). Interpretation 8 (4), SQ15–SQ24. https://doi.org/10.1190/INT-2020-0026.1.
ICGC, 2016. Mapa geològic comarcal 1:50.00.
Izquierdo-Llavall, E., Casas-Sainz, A.M., Oliva-Urcia, B., 2013. Heterogeneous deformation recorded by magnetic fabrics in the Pyrenean Axial Zone. J. Struct. Geol. 57, 97–113. https://doi.org/10.1016/j.jsg.2013.10.005.
Izquierdo-Llavall, E., Menant, A., Aubourg, C., Callot, J.P., Hoareau, G., Camps, P., Lahfid, A., 2020. Preorogenic folds and syn-orogenic basement tilts in an inverted hyperextended margin: the Northern Pyrenees case study. Tectonics 39 (7) e2019TC005719.
Kleinsmiede, W.F.J., 1960. Geology of the Valle d'Aran (Central Pyrenees). Leidse. Geol. Meded. 25, 129–245.
Lanaja, J.M. (Ed.), 1987. Contribución de la exploración petrolífera al conocimiento de la geología de España. IGME, Madrid.
Le Pape, F., Jones, A.G., Jessell, M.W., Perrouty, S., Gallardo, L.A., Baratoux, A., Hogg, C., Siebenaller, L., Touré, A., Ouiya, P., Boren, G., 2017. Crustal structure of southern Burkina Faso inferred from magnetotelluric, gravity and magnetic data. Precambrian Res. 300, 261–272. ISSN 0301–9268. https://doi.org/10.1016/j.precamres.2017.08.013.
Leblanc, D., Gleizes, G., Lespinasse, P., Olivier, P.H., Bouchez, J.L., 1994. The Maladeta granite polydiapir, Spanish Pyrenees: a detailed magnetostructural study. J. Struct. Geol. 16-2, 223–235. ISSN 0191–8141. https://doi.org/10.1016/0191-8141(94)90106-6.
Ledo, J., Jones, A.G., 2005. Upper mantle temperature determined from combining mineral composition, electrical conductivity laboratory studies and magnetotelluric field observations: application to the intermontane belt, Northern Canadian Cordillera. Earth Planet. Sci. Lett. 236 (1–2), 258–268. https://doi.org/10.1016/j.epsl.2005.01.044.
Ledo, J., Ayala, C., Pous, J., Queralt, P., Marcuello, A., Munoz, J.A., 2000. New geophysical constraints on the deep structure of the Pyrenees. Geophys. Res. Lett. 27 (7), 1037–1040. https://doi.org/10.1029/1999GL011005.
López-Olmedo, F., Ardèvol, L., 2016. Mapa Geológico de España E. 1:50.000, Hoja no 251 (Arén), 2ª Serie MAGNA. Instituto Geológico y Minero de España, Madrid.
López-Sánchez, M., García-Sansegundo, J., Martínez, F., 2019. The significance of early Permian and early Carboniferous U-Pb zircon ages in the Bossòst and Lys-Caillaouas granitoids (Pyrenean Axial Zone). Geol. J. 54 (4), 2048–2063. https://doi.org/10.1002/gj.3283.
Marcén, M., Casas-Sainz, A.M., Román-Berdiel, T., Oliva-Urcia, B., Soto, R., Aldega, L., 2018. Kinematics and strain distribution in anorogen-scale shear zone: insights from structural analyses and magnetic fabrics in the Gavarnie thrust, Pyrenees. J. Struct. Geol. 117, 105–123.
Matte, P., 1969. Le probleme du passage de la schistosit. horizontala la schistosit. verticale dans la d.me de la Garonne (Paléozoique des Pyrénées Centrales). C. R. Acad. Sci. 268, 1841–1844.
McNeice, G.W., Jones, A.G., 2001. Multisite, multifrequency tensor decomposition of magnetotelluric data. Geophysics 66 (1), 158–173.
Mencos, J., Carrera, N., Muñoz, J.A., 2015. Influence of rift basin geometry on the subsequent postrift sedimentation and basin inversión: the Organyà Basin and the Bóixols thrust sheet (south Central Pyrenees). Tectonics 34 (7), 1452–1474. https://doi.org/10.1002/2014TC003692.
Michard-Vitrac, A., Albarede, F., Dupuis, C., Taylor, H.P., 1980. The genesis of Variscan (Hercynian) plutonic rocks: Inferences from Sr, Pb, and O studies on the Maladeta igneous complex, Central Pyrenees (Spain). Contrib. Mineral. Petrol. 72 (1), 57–72.
Mitjanas, G., Ledo, J., Macau, A., Alías, G., Queralt, P., Bellmunt, F., Rivero, Ll., Gabàs, A., Marcuello, A., Benjumea, B., Martí, A., Figueras, S., 2021. Integrated seismic ambient noise, magnetotellurics and gravity data for the 2D interpretation of the Vallès basin structure in the geothermal system of La Garriga-Samalús (NE Spain). Geothermics 93, 102067. ISSN 0375-6505,. https://doi.org/10.1016/j.geothermics.2021.102067.
Mouthereau, F., Filleaudeau, P.Y., Vacherat, A., Pik, R., Lacombe, O., Fellin, M.G., Masini, E., 2014. Placing limits to shortening evolution in the Pyrenees: role of margin architecture and implications for the Iberia/Europe convergence. Tectonics 33 (12), 2283–2314.
Muñoz, J.A., 1992. Evolution of a continental collision belt: ECORS Pyrenees crustal balanced cross-section. In: McClay, K.R. (Ed.), Thrust Tectonics. Chapman and Hall, London, pp. 235–246.
Muñoz, J.A., Mencos, J., Roca, E., Carrera, N., Cratacós, O., Ferrer, O., Fernández, O., 2018. The structure of the South-Central-Pyrenean fold and thrust belt as constrained by subsurface data. Geol. Acta 16 (4), 439–460. https://doi.org/10.1344/GeologicaActa20 18.16.4.7.
Olivier, P., Améglio, L., Richen, H., Vadeboin, F., 1999. Emplacement of the Aya Variscan granitic pluton (Basque Pyrenees) in a dextral transcurrent regime inferred from a combined magneto-structural and gravimetric study. J. Geol. Soc. Lond. 156, 991–1002.
Ortuño, M., Queralt, P., Martí, A., Ledo, J., Masana, E., Perea, H., Santanach, P., 2008. The North Maladeta Fault (Spanish Central Pyrenees) as the Vielha 1923 earthquake seismic source: recent activity revealed by geomorphological and geophysical research. Tectonophysics 453, 246–262.
Ortuño, M., Martí, A., Martín-Closas, C., Jiménez-Moreno, G., Martinetto, E., Santanach, P., 2013. Palaeoenvironments of the late Miocene Prüedo Basin: implications for the uplift of the Central Pyrenees. J. Geol. Soc. 170, 79–92. https://doi.org/10.1144/jgs2011-121.
Piña-Varas, P., Ledo, J., Queralt, P., et al., 2018. On the detectability of Teide volcano magma chambers (Tenerife, Canary Islands) with magnetotelluric data. Earth Planets Space 70, 14. https://doi.org/10.1186/s40623-018-0783-y.
Poblet, J., 1991. Estructura herciniana i alpina del Vessant sud de la zona Axial del Pirineu Central. Unpublished PhD thesis,. Univ. of Barcelona, p. 604.
Pous, J., Ayala, C., Ledo, J., Marcuello, A., Sàbat, F., 1995. 3D modelling of magnetotelluric and gravity data of Mallorca Island (western Mediterranean). Geophys. Res. Lett. 22 (6), 735–738. https://doi.org/10.1029/95GL00271.
Pujalte, V., Schmitz, B., 2005. Revisión de la estratigrafía del Grupo Tremp («Garumniense», Cuenca de Tremp-Graus, Pirineos meridionales). Geogaceta 38, 79–82.
Ríos-Aragües, L.M., Galera-Fernández, J.M., Barettino, D., Charlet, J.M., 2002. Mapa Geológico de España E. 1:50.000, Hoja n° 180 (Benasque), 2ª Serie MAGNA. Instituto Geológico y Minero de España, Madrid.
Rodi, W., Mackie, R.L., 2001. Nonlinear conjugate gradients algorithm for 2-Dmagnetotelluric inversion. Geophysics 66 (1), 174–187. https://doi.org/10.1190/1.1444893.
Rodríguez, F., Pérez, N.M., Padrón, E., Melián, G., Hernández, P.A., Asensio-Ramos, M., Dionis, S., López, G., Marrero, R., Padilla, G.D., et al., 2015. Diffuse helium and hydrogen degassing to reveal hidden geothermal resources in oceanic volcanic islands: the Canarian archipelago case study. Surv. Geophys. 36 (3), 351–369.
Rosell, J., 1994. Mapa Geológico de España E. 1:50.000, Hoja n° 252 (Tremp), 2ª Serie MAGNA. Instituto Geológico y Minero de España, Madrid.
Roure, F., Choukroune, P., Berastegui, X., Munoz, J.A., Villien, A., Matheron, P., Deramond, J., 1989. ECORS deep seismic data and balanced cross sections: Geometric constraints on the evolution of the Pyrenees. Tectonics 8 (1), 41–50.
Rubinat, M., Ledo, J., Roca, E., Rosell, O., Queralt, P., 2010. Magnetotelluric characterization of a salt diapir: a case study on Bicorb–Quesa Diapir (Prebetic Zone, SE Spain). J. Geol. Soc. 167 (1), 145–153. https://doi.org/10.1144/0016-76492009-029.
Santolaria, P., Casas-Sainz, A.M., Soto, R., Casas, A., 2016. Gravity modelling to assess salt tectonics in the western end of the South Pyrenean Central Unit. J. Geol. Soc. 174, 269–288. https://doi.org/10.1144/jgs20 16- 027.
Saura, E., Ardévol, L.I., Teixell, A., Vergés, J., 2016. Rising and falling diapirs, shifting depocenters and fap overturning in the cretaceous Sopeira and Sant Gervàs subbasins (Ribagorça basin, Pyrenees). Tectonics 35, 638–662.
Schnapperelle, S., Mezger, J.E., Stipp, M., Hofmann, M., Gärtner, A., Linnemann, U., 2020. Polyphase magmatic pulses along the Northern Gondwana margin: U-Pb zircon geochronology from gneiss domes of the Pyrenees. Gondwana Res. 81, 291–311.
Seguret, M., 1972. Étude tectonique des nappes et séries décollées de la partie centrale du versant sud des Pyrénées. Pub. Estela. Ser. Geol. Struct. 2, 1–155.
Simó, A., 2004. El Cretácico superior de la Unidad Surpirenaica central. In: Vera, J.A. (Ed.), Geología de España. Sociedad Geológica de España-Instituto Geológico y Minero de España, pp. 296–299.
Solé, J., Soler, A., Palau, J., Espinola, M.R., Delgado, J., 1997. Geocronología K/Ar de los skarns mineralizados en As-Au y de las alteraciones intragraníticas asociadas en el Hercínico de los Pirineos Centrales [abs.]. Bol. Soc. Esp. Mineral. 20-A, 77–78.
Soto, R., Clariana, P., Ayala, C., Rey-Moral, C., Casas-Sainz, A.M., Román-Berdiel, T., et al., 2022. Assessing the internal uppermost crustal structure of the Central Pyrenees by gravity-constrained cross sections. Tectonics 41. https://doi.org/10.1029/2021TC007009 e2021TC007009.
Talwani, M., Worzel, J.L., Landisman, M., 1959. Rapid gravity computations for two dimensional bodies with application to the Mendocino submarine fracture zone. J. Geophys. Res. 64 (1), 49–59. https://doi.org/10.1029/JZ064i001p00049.
Teixell, A., Muñoz, J.A., 2000. Evolución tectono-sedimentaria del Pirineo meridional durante el Terciario: una síntesis basada en la transversal del río Noguera Ribagorçana. Rev. Soc. Geol. Esp. 13, 295–316.
Teixell, A., Labaume, P., Ayarza, P., Espurt, N., Saint Blanquat, M., Lababrielle, Y., 2018. Crustal structure and evolution of the Pyrenean Cantabrian belt: a review and new interpretations from recent concepts and data. Tectonophysics 724–725, 146–170. https://doi.org/10.1016/j.tecto.2018.01.009.
Torné, M., Fernàndez, M., Vergés, J., Ayala, C., Salas, M.C., Jimenez-Munt, Y., Buffet, G. G., Díaz, J., 2015. Crust and mantle lithospheric structure of the Iberian Peninsula deduced from potential field modeling and thermal analysis. Tectonophysics 663, 419–433.
Ubide, T., Wijbrans, J.R., Galé, C., Arranz, E., Lago, M., Larrea, P., 2014. Age of the cretaceous alkaline magmatism in Northeast Iberia: Implications for the Alpine cycle in the Pyrenees. Tectonics 3 (7), 0278–7407. https://doi.org/10.1002/2013TC003511.
Waldner, M., Bellahsen, N., Mouthereau, F., Bernet, M., Pik, R., Rosenberg, C.L., Balvay, M., 2021. Central Pyrenees mountain building: constraints from new LT thermochronological data from the Axial Zone. Tectonics 40. https://doi.org/10.1029/2020TC006614 e2020TC006614.
Wang, Y., Chevrot, S., Monteiller, V., Komatitsch, D., Mouthereau, F., Manatschal, G., et al., 2016. The deep roots of the western Pyrenees revealed by full waveform inversion of teleseismic P waves. Geology 44 (6), 475–478. https://doi.org/10.1130/g37812.1.
Won, I.J., Bevis, M., 1987. Computing the gravitational and magnetic anomalies due to a polygon: Algorithms and Fortran subroutines. Geophysics 52 (2), 232–238. https://doi.org/10.1190/1.1442298.
Zwart, H.J., 1979. The geology of the central Pyrenees. Leidse Geol. Meded. Deel 50. Aflevering I. 1-74, 1-11.